Three-dimensional Marangoni–Bénard flows in square and nearly square containers

A. Bergeon[a)]
U.M.R. 5502 IMFT-CNRS-UPS, U.F.R. M.I.G., 31062 Toulouse Cedex, France

D. Henry
U.M.R. C.N.R.S. 5509, LMFA-ECL-UCB, BP 163, 69131 Ecully Cedex, France

E. Knobloch
Department of Physics, University of California, Berkeley, California 94720

(Received 13 January 2000; accepted 20 September 2000)

Numerical continuation is used to follow branches of steady solutions to the three-dimensional Marangoni–Bénard problem in a zero gravity environment. The upper surface of the fluid is heated by a constant heat flux while the bottom is maintained at a constant temperature. Instability arises due to temperature-dependent surface tension effects but surface deflection is ignored. Containers with square and nearly square cross sections and no-slip boundary conditions are analyzed, and the results interpreted in terms of predictions from equivariant bifurcation theory. © *2001 American Institute of Physics.* [DOI: 10.1063/1.1329905]

I. INTRODUCTION

The term Marangoni–Bénard convection refers to flows induced by surface tension gradients created by variations of temperature along the free surface of a fluid placed in a vertical temperature gradient. Such flows have a significant influence on many industrial processes such as those involving solidification from a molten alloy[1] and are particularly important in a zero gravity environment.

We consider a one-component incompressible fluid in a three-dimensional container open at the top, the bottom of which $(z=0)$ is maintained at a constant temperature T_0. A constant normal heat flux $-q>0$ is applied (in the downward direction) at the free upper surface located at $z=H$. The velocity is taken to vanish along the walls, assumed to be no-slip, and the lateral walls, located at $x=\pm L_x/2$, $y=\pm L_y/2$, are considered to be adiabatic. The surface tension at the free upper surface is assumed to vary linearly with the surface temperature: $\sigma(T)=\sigma_0(1+\gamma_T(T-T_0))$, where σ_0 is a constant. The surface itself is assumed to remain undeformed by the flow (σ is large), and the gas in contact with it to have no influence. The conditions for stress equilibrium along the free surface then are

$$\rho\nu\frac{\partial u}{\partial z}=\sigma_0\gamma_T\frac{\partial T}{\partial x},\quad \rho\nu\frac{\partial v}{\partial z}=\sigma_0\gamma_T\frac{\partial T}{\partial y}, \tag{1}$$

where $\mathbf{u}\equiv(u,v,w)$ is the velocity in the (x,y,z) coordinates, ρ is the density of the fluid, and ν is its kinematic viscosity. This condition is responsible for the onset of convection. The conduction state $\mathbf{u}=\mathbf{0}$, $T=T_c(z)$ is destabilized by temperature fluctuations along the upper surface when the imposed heat flux $-q$ exceeds a critical value as measured by the flux Marangoni number $\mathrm{Ma}\equiv -qH^2\sigma_0\gamma_T/\lambda\rho\nu\kappa$, cf. Ref. 2. Here κ is the thermal diffusivity and $\lambda\equiv C_V\rho\kappa$ is the thermal conductivity. For fluids with $\gamma_T<0$ the above formulation remains valid provided the sign of q is reversed, i.e., provided the surface is cooled instead of being heated.

In the following, distance, time, temperature, and velocity are nondimensionalized using H, H^2/ν, $\Delta T\equiv -qH/\lambda$, and $\mathrm{Ma}\,\nu/H$, respectively. Thus $A_x\equiv L_x/H$, $A_y\equiv L_y/H$ are the horizontal aspect ratios of the container. In zero gravity the dimensionless equations for $\mathbf{u}$, p, and T are

$$\partial_t\mathbf{u}=-\mathrm{Ma}(\mathbf{u}\cdot\boldsymbol{\nabla})\mathbf{u}-\boldsymbol{\nabla}p+\boldsymbol{\nabla}^2\mathbf{u},\quad \boldsymbol{\nabla}\cdot\mathbf{u}=0, \tag{2}$$

$$\partial_t T=-\mathrm{Ma}(\mathbf{u}\cdot\boldsymbol{\nabla})T+\mathrm{Pr}^{-1}\boldsymbol{\nabla}^2T, \tag{3}$$

where $\mathbf{u}$, p, T, x, y, z, and t now refer to dimensionless variables, and $\mathrm{Pr}=\nu/\kappa$ is the Prandtl number. The boundary conditions along the free surface $(z=1)$ are

$$\partial_z u-\partial_x T=\partial_z v-\partial_y T=w=\partial_z T-1=0, \tag{4}$$

while those along the bottom $(z=0)$ are $\mathbf{u}=T=0$. Along the lateral walls $(x=\mp A_x/2$ or $y=\mp A_y/2)$ we have $\mathbf{u}=\partial_n T=0$, where n is the coordinate normal to the wall. Consequently, the pure conduction state $[\mathbf{u}=0,\ T(z)=z]$ is a solution of the problem for any Marangoni number Ma. In this article we focus on containers with a square or almost square horizontal cross-section $(A_x\approx A_y)$ and relatively small aspect ratio $(A_x\approx 1.5)$. In this regime Rosenblat *et al.*[2] predict, for Neumann sidewall boundary conditions, that convection will take the form of a single roll state, oriented parallel to the short side.

More recent work on the problem has employed the more realistic boundary conditions specified earlier, and investigated not only the onset of the instability but also the structure of the resulting nonlinear flow, both in two and three dimensions.[3–8] The primary purpose of the present ar-

[a)]Author to whom correspondence should be addressed: Université Paul Sabatier UFR MIG-IMFT UMR CNRS 5502, Dépt. Mécanique Bat. 1R2, 118, route de Narbonne, 31062 Toulouse, France. Electronic mail: bergeon@lm2f.ups-tlse.fr

ticle is to apply numerical branch following algorithms to the three-dimensional problem, and to elucidate the complete bifurcation structure of the problem for aspect ratios for which the solution multiplicity is still relatively small. We show that, in these relatively simple cases, the qualitative features of the computed bifurcation diagrams for a square and nearly square container can be understood in all respects using simple ideas from group theory. The results indicate graphically the sensitivity of the bifurcation diagrams to small changes in the symmetry of the container, contrary to the basic premise of Ref. 5.

Symmetries enter into problems of this type from the invariance properties of the governing equations and the shape of the container. In two dimensions the relevant symmetry is the group $\mathbf{Z}_2$, generated by the reflection $\mathcal{S}_x$ in the vertical plane $x=0$. For three-dimensional containers with $A_x \neq A_y$ the symmetry group is generated by two such reflections, $\mathcal{S}_x$ and $\mathcal{S}_y$, and is therefore $\mathbf{Z}_2 \times \mathbf{Z}_2 \equiv \mathbf{D}_2$. In the particular case $A_x = A_y$ there are additional reflection symmetries, Π_{xy} and Π_{yx}, with respect to the vertical planes along the two diagonals. In this case the symmetry group is the dihedral group $\mathbf{D}_4$ generated by $\mathcal{S}_x$ and Π_{xy}. This is the symmetry group of a square. Note that while the two generators are both reflections they do not commute with each other. Consequently the group $\mathbf{D}_4$ contains eight elements. In contrast, when the relevant reflections do commute the resulting group is $\mathbf{D}_2$ and contains only four elements. The structure of the group has important consequences even for the linear stability problem of the conduction state, at least when the unstable mode breaks the symmetry of this state. Likewise, symmetries restrict the possible secondary bifurcations from nontrivial (i.e., convecting) states whenever these are themselves symmetric. In each case the role played by the symmetry group depends on its action on the marginal eigenfunction. Consequently, the same symmetry group will have different consequences for different bifurcations.

In the following we compute numerically the bifurcation diagrams for both the $\mathbf{D}_4$ (square base) and $\mathbf{D}_2$ (rectangular base) cases, using a spectral method for the spatial discretization of the conservation laws.[9] A first-order time-stepping code[10] is adapted for finding steady states as described by Tuckerman,[11] Mamun and Tuckerman,[12] and Bergeon *et al.*[8] The solver is incorporated into a standard continuation method by which branches of steady states are followed as a function of the Marangoni number. During the continuation procedure, we occasionally compute some of the leading eigenvalues and their eigenvectors using an adaptation of Arnoldi's method described in Ref. 12. As a result we locate the interval in the Marangoni number in which a steady or a Hopf bifurcation is present but not the bifurcation point itself. In fact in the present problem no Hopf bifurcations were detected. On the other hand, once a steady bifurcation is located, the corresponding unstable eigenvector and the associated steady state are used to build a predictor for a solution along the emerging branch; the code then uses continuation to follow the new branch. Since the exact computation of secondary bifurcation points is not performed, the critical parameter values are obtained from the intersection of the two branches involved. This continuation procedure was used to obtain Figs. 1, 3, 4, 5, and 7; in contrast, the primary bifurcations and the corresponding eigenvectors shown in Figs. 2 and 6 were obtained by solving directly the nonlinear system for the bifurcation point. Details and validations of the method are given in Refs. 8 and 13.

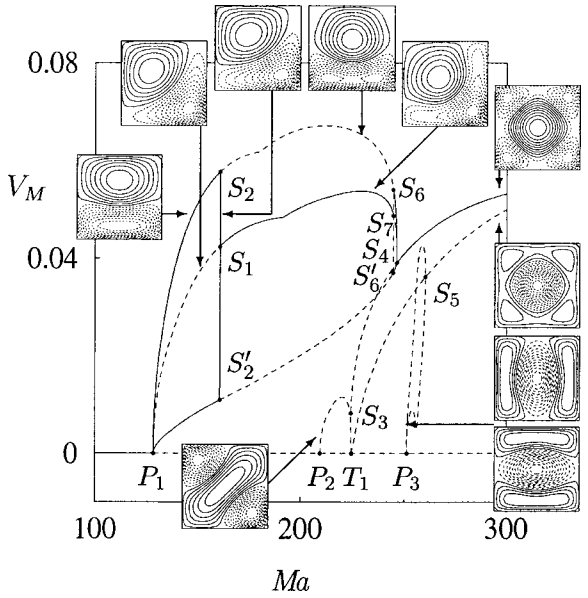

FIG. 1. Bifurcation diagram for $A_x = A_y = 1.5$ and Pr=0.6 (see text for explanation). The resolution is $13 \times 13 \times 11$.

To check the accuracy of the code, we computed parts of the bifurcation diagram in Fig. 1 ($A_x = A_y = 1.5$), increasing the resolution until no significant difference was detected. As an additional check, the values obtained for the primary bifurcation points from the intersections of the nontrivial solution branches with the trivial branch (Figs. 1, 4, 5, and 7) were compared with the results of the direct computation of the primary bifurcation points used for Figs. 2 and 6. Very good agreement was found in all instances. All the calculations in this article use Pr=0.6.

II. SQUARE CONTAINER

Figure 1 shows the bifurcation diagram for the $\mathbf{D}_4$ case with $A_x = A_y = 1.5$, hereafter $A = 1.5$. The figure displays the evolution with the Marangoni number of the maximum V_M of the y velocity component v measured at the Gauss–Lobatto–Legendre nodes.[14] Consequently, large values of V_M indicate x-rolls (i.e., rolls with axes parallel to the x direction,[15] shown as horizontal in the insets) while small values of V_M indicate y-rolls (rolls with axes parallel to the y direction, shown as vertical in the insets); the value $V_M = 0$ corresponds to the conduction state. The flows corresponding to different locations on each branch are depicted through isovalues of the vertical velocity w in the horizontal midplane $z = \frac{1}{2}$; these indicate the symmetry of the branch. Since the symmetry cannot change along solution branches except at bifurcation points we refer to each branch by the symmetry of the solutions on that branch. Continuous lines denote linearly stable steady solutions while dashed lines denote steady solutions that are at least once linearly unstable. The conduction state $V_M = 0$ is stable up to $\mathrm{Ma}_{P_1} = 127.86$ corre-

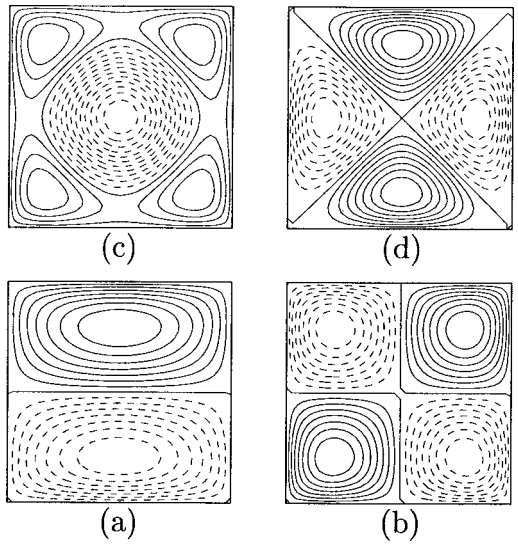

FIG. 2. Critical vertical velocity eigenfunctions at the primary bifurcation points P_1, P_2, T_1, and P_3 for $A_x=A_y=1.5$ with (a) $\mathrm{Ma}_{P_1}=127.86$ ($\mathbf{Z}_2$-symmetric, fixed by $\mathcal{S}_x$), (b) $\mathrm{Ma}_{P_2}=204.3$ ($\mathbf{D}_2$-symmetric, fixed by Π_{xy} and Π_{yx}), (c) $\mathrm{Ma}_{T_1}=224.1$ ($\mathbf{D}_4$-symmetric, fixed by $\mathcal{S}_x$ and Π_{xy} and their products), and (d) $\mathrm{Ma}_{P_3}=248.6$ ($\mathbf{D}_2$-symmetric, fixed by $\mathcal{S}_x$ and $\mathcal{S}_y$). The symmetry of the eigenfunction (a) indicates that P_1 corresponds to a double zero eigenvalue: $\pi/2$ rotation of (a) about $x=y=0$ generates an independent eigenfunction. The resolution is $N_x\times N_y\times N_z=15\times15\times13$.

sponding to the point P_1 in Fig. 1. At this point *two* eigenvalues pass through zero. Additional (simple) eigenvalues cross zero at $\mathrm{Ma}_{P_2}=204.3$, $\mathrm{Ma}_{T_1}=224.1$, and $\mathrm{Ma}_{P_3}=248.6$. The corresponding eigenfunctions are shown in Fig. 2; these help us understand[16–18] various aspects of the bifurcation diagram in Fig. 1, and indicate that four of the five[19] irreducible representations of the group $\mathbf{D}_4$ appear in this problem in successive bifurcations. As such the present problem provides an excellent illustration of the type of symmetry argument that sheds much light on the observed transitions.

Figure 1 reveals that at P_1 three solution branches bifurcate simultaneously from the conduction state. Of these, two (corresponding to *x*-rolls and *y*-rolls) are initially stable, while the third, corresponding to an equal amplitude superposition of *x*- and *y*-rolls, is unstable. Note that the quantity V_M distinguishes between *x*-rolls and *y*-rolls even though these are related by a reflection in the diagonal, but that it does not distinguish between solutions with Π_{xy} and Π_{yx} symmetries. The multiplicity of branches emerging from P_1 is a consequence of the symmetry of the eigenfunction (a) of Fig. 2. This eigenfunction, corresponding to an *x*-roll and denoted hereafter $f_{P_1}(x,y,z)$, is symmetric under $\mathcal{S}_x$ but breaks all the other symmetries in $\mathbf{D}_4$. Thus the general solution of the linear stability problem at P_1 takes the form $w(x,y,z,t)=a_1(t)f_{P_1}(x,y,z)+a_2(t)f_{P_1}(y,x,z)$, where $a_1(t)$ and $a_2(t)$ are the (real) amplitudes of *x*-rolls and *y*-rolls, respectively (cf. Ref. 15). Near P_1 the nonlinear solution will resemble the linear solution, provided this solution respects the symmetries of the system, i.e., provided the application of the symmetry operations in $\mathbf{D}_4$ generates other solutions of the equations. This requires that the equations

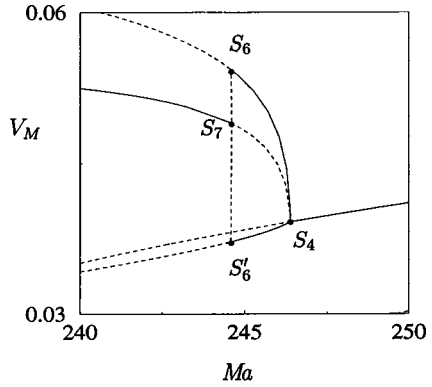

FIG. 3. Enlargement of the region in Fig. 1 near S_4.

for the amplitudes commute with the two operations that generate $\mathbf{D}_4$:

$$\mathcal{S}_x\cdot(a_1,a_2)=(a_1,-a_2),\quad \Pi_{xy}\cdot(a_1,a_2)=(a_2,a_1). \tag{5}$$

Thus, cf. Ref. 16,

$$\dot{a}_1=g(\lambda,a_1^2,a_2^2)a_1,\quad \dot{a}_2=g(\lambda,a_2^2,a_1^2)a_2, \tag{6}$$

where g is a C^∞ real-valued function and λ is the threshold distance $(\mathrm{Ma}-\mathrm{Ma}_{P_1})/\mathrm{Ma}_{P_1}$. These equations are the normal form for the steady-state bifurcation with $\mathbf{D}_4$ symmetry analyzed in Refs. 16–18. In the generic case these equations have only two types (modulo symmetry-related states) of nontrivial solutions near the origin, $\mathcal{S}_x$-symmetric states $(a_1,a_2)=(a,0)$ and Π_{xy}-symmetric states $(a_1,a_2)=(a,a)$, both of which bifurcate simultaneously from (0,0) at $\lambda=0$, in agreement with Fig. 1. Moreover, the cubic truncation

$$\begin{aligned}\dot{a}_1&=(\lambda+\alpha a_2^2+\beta(a_1^2+a_2^2))a_1,\\ \dot{a}_2&=(\lambda+\alpha a_1^2+\beta(a_1^2+a_2^2))a_2,\end{aligned} \tag{7}$$

shows that the former are stable when $\alpha<0$, $\beta<0$ while the latter are stable when $\alpha>0$, $\alpha+2\beta<0$. When $\alpha=0$ these solutions are degenerate in the sense that one of their eigenvalues (the one that describes their stability with respect to perturbations in the form of the other) vanishes. The unfolding of this degeneracy contains a secondary branch of *nonsymmetric* solutions. Knobloch[20] points out that in order to determine correctly the stability properties of this branch the function g must be expanded to *sixth* order in the amplitudes.[21] We have not computed the necessary coefficients, but note that there are just two possibilities, either the secondary branch $S_2S_1S_2'$ is supercritical and stable as in Fig. 1 or it bifurcates subcritically and is unstable. In the former case the transfer of stability from the $\mathcal{S}$-symmetric states (i.e., states invariant under either $\mathcal{S}_x$ or $\mathcal{S}_y$) to the Π-symmetric states (i.e., states invariant under either Π_{xy} or Π_{yx}) occurs without hysteresis, while in the latter case it is hysteretic. The latter possibility is found near S_4, as indicated by the dashed curve $S_6S_7S_6'$ in Fig. 3. At this point a $\mathbf{D}_4$-symmetric solution undergoes a symmetry-breaking bifurcation that produces $\mathcal{S}$-symmetric states. Consequently, the above theory applies, and shows that two distinct solution types must emerge from S_4, solutions with $\mathcal{S}$ symmetry and solutions with Π symmetry. The former are again stable

and the latter unstable. However, this time the nonsymmetric branch $S_6S_7S_6'$ is unstable and the transfer of stability between the $\mathcal{S}$- and Π-symmetric branches is therefore hysteretic. Note that despite appearances neither $S_2S_1S_2'$ nor $S_6S_7S_6'$ is actually vertical.

Additional primary bifurcations occur at larger Marangoni numbers. At P_2 the conduction state loses stability to a $\mathbf{D}_2$-symmetric state, invariant under both Π_{xy} and Π_{yx}. Since neither generator of $\mathbf{D}_4$ produces an independent eigenfunction from $f_{P_2}(x,y,z)$ the associated zero eigenvalue is simple. Moreover, since $\mathcal{S}_x$ changes the sign of $f_{P_2}(x,y,z)$ the resulting bifurcation is a pitchfork. In contrast the bifurcation at T_1 preserves the $\mathbf{D}_4$ symmetry and is therefore a generic steady state bifurcation. Since the conduction state is a solution for all Ma this bifurcation is transcritical and the emerging solutions $\mathbf{D}_4$-symmetric. Figure 1 shows that the supercritical part of this branch corresponds to flows in which the fluid rises towards the free surface along the lateral sides of the container, while the subcritical part corresponds to flows in which the fluid rises towards the free surface in the center. Finally, the bifurcation at P_3 also breaks the $\mathbf{D}_4$ symmetry but in this case the corresponding eigenfunction $f_{P_3}(x,y,z)$ is invariant under both $\mathcal{S}_x$ and $\mathcal{S}_y$ while Π_{xy} and Π_{yx} act by -1. The corresponding eigenvalue is therefore simple and the bifurcation is again a pitchfork.

We next turn to the secondary bifurcations. Of these the bifurcations at S_1 and S_7 are pitchforks because the solutions are Π-symmetric and this symmetry is in both cases broken at the bifurcation. The branches emerging from P_1, P_2, and P_3 all terminate at secondary bifurcation points on the branches of $\mathbf{D}_4$-symmetric solutions, with S_3 and S_4 on the subcritical part and S_5 on the supercritical part. Thus S_3, S_4, and S_5 are also steady-state bifurcations with $\mathbf{D}_4$ symmetry. Of these, the bifurcation at S_4 has already been discussed. Examination of Fig. 1 indicates that the remaining bifurcations break $\mathbf{D}_4$ down to $\mathbf{D}_2$ and hence correspond to simple eigenvalues, with S_3 like P_2 and S_5 like P_3. Both are pitchforks. As a result of these connections, the subcritical $\mathbf{D}_4$-symmetric branch (which is four times unstable close to T_1 and three times unstable after a saddle-node bifurcation below S_3) acquires stability beyond S_4. We note that the branches created at P_1 and P_2 form closed curves, a phenomenon also observed in two-dimensional containers.[3,8]

III. SLIGHTLY RECTANGULAR CONTAINERS

We next describe what happens when the container is slightly rectangular, i.e., how Fig. 1 unfolds when the symmetry of the problem changes from $\mathbf{D}_4$ to $\mathbf{D}_2$. We expect that such a change in symmetry will have different effects in different parts of the bifurcation diagram in Fig. 1, depending on the symmetry involved in the various primary and secondary bifurcations. In particular we expect all double multiplicity zero eigenvalues to split. Figures 4 and 5 show what happens when $A_x=1.501$ and $A_y=1.5$. Figure 4 shows that the bifurcation at P_1 is indeed split into two successive pitchfork bifurcations, now called P_1' and P_1, the first of which produces a branch of stable *y*-rolls and the second a branch of unstable *x*-rolls. This splitting occurs because the

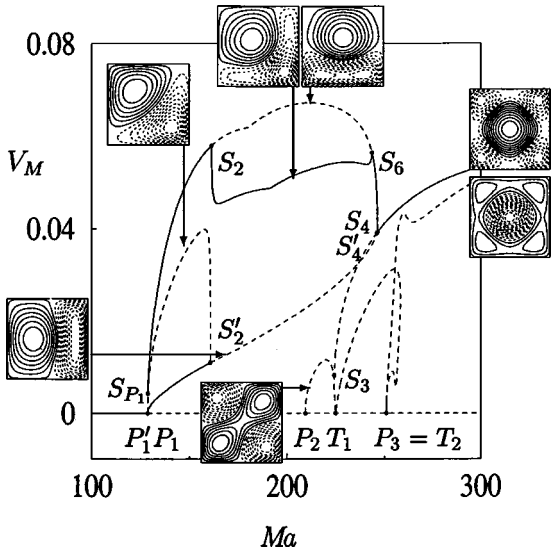

FIG. 4. Bifurcation diagram for $A_x=1.501$ and $A_y=1.5$. The resolution is $13\times13\times11$.

two eigenfunctions (a,b) of Fig. 6 are no longer related by the symmetry Π_{yx}; the preference for *y*-rolls is reminiscent of the corresponding results for Rayleigh–Bénard convection.[15] However, in the present problem the situation is more complex. This is because two competing factors are important. When A_x increases for fixed A_y the threshold Marangoni number for the onset of *x*-rolls drops monotonically because the confining effect of the transverse walls gradually decreases. At the same time the choice of A_y imposes a wavelength on the *x*-rolls, and this results in a neutral curve that falls off with A_y in an oscillatory fashion with minima near values of A_y favoring the natural wavelength of the rolls. As a result there are parameters for which the first instability is in fact to rolls parallel to the long side of the container.[5] This is the case, for example, when $A=1.6$.

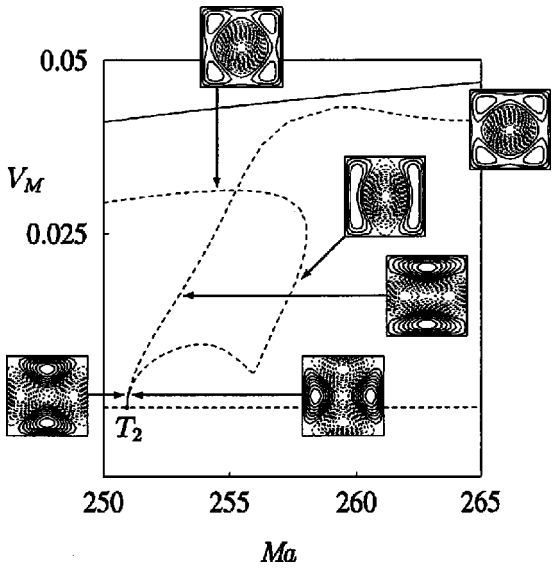

FIG. 5. Bifurcation diagram for $A_x=1.501$ and $A_y=1.5$: enlargement of the region in Fig. 4 near T_2. The resolution is $13\times13\times11$.

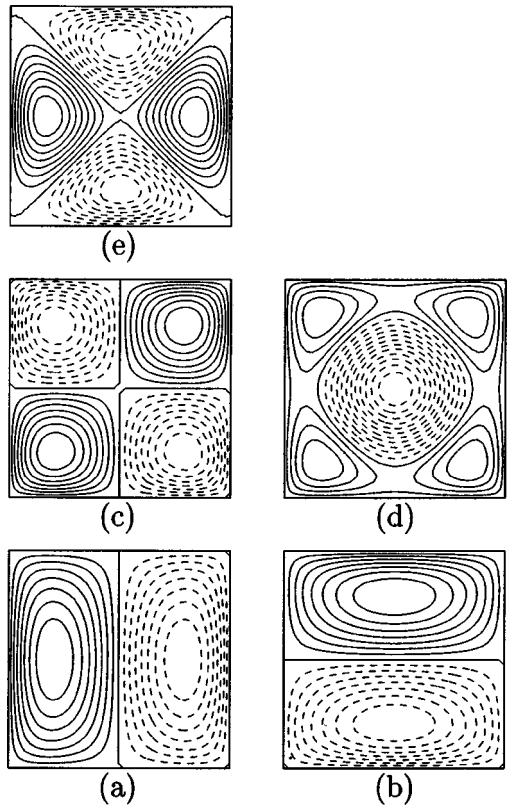

FIG. 6. Critical eigenfunctions at the primary bifurcation points P_1', P_1, P_2, T_1 and $P_3=T_2$ for $A_x=1.501$ and $A_y=1.5$ with (a) $\mathrm{Ma}_{P_1'}=127.82$, (b) $\mathrm{Ma}_{P_1}=127.83$, (c) $\mathrm{Ma}_{P_2}=204.2$, (d) $\mathrm{Ma}_{T_1}=224.0$, and (e) $\mathrm{Ma}_{T_2}=248.5$. The resolution is $N_x\times N_y\times N_z=15\times 15\times 13$.

In the nonlinear regime both roll branches undergo stability-changing secondary bifurcations with increasing Ma. At S_2' the *y*-rolls lose stability to perturbations in the form of *x*-rolls, producing a secondary branch of solutions that resemble *y*-rolls near S_2' and gradually change into an almost Π-symmetric state (see inset) before becoming *x*-rolls at S_{P_1}. At S_{P_1} the branch of *x*-rolls acquires stability. It loses it again at S_2 where another secondary branch of nonsymmetric states appears. These resemble *x*-rolls near S_2, and evolve towards Π-symmetric states before becoming *x*-rolls again at S_6. Thus in the rectangular container the branch corresponding to the Π-symmetric states is no longer a primary branch and, moreover, breaks up into disconnected pieces. This behavior is easy to understand using the unfolding[22] of Eqs. (7),

$$\dot{a}_1=(\lambda-\epsilon+\alpha a_2^2+\beta(a_1^2+a_2^2))a_1,$$
$$\dot{a}_2=(\lambda+\alpha a_1^2+\beta(a_1^2+a_2^2))a_2. \tag{8}$$

Here $0<\epsilon\ll 1$ measures the departure from square cross section, i.e., $\epsilon\propto(A_x-A_y)/A_x$. Equations (8) can be used to show that the only primary bifurcations are to *y*-rolls (at $\lambda=0$) or to *x*-rolls (at $\lambda=\epsilon$), as in Fig. 4. Moreover, in the case in which rolls are stable and the Π states unstable at $\epsilon=0$, there is necessarily a secondary bifurcation to an unstable Π-like state on one of the roll branches close to the primary bifurcation. In fact, a detailed analysis[23] of the effects of breaking the $\mathbf{D}_4$ symmetry down to $\mathbf{D}_2$ on the degeneracy $\alpha=0$ shows that the pitchfork at S_1 in Fig. 1 must unfold according to the universal unfolding of the pitchfork bifurcation.[24] The disconnected branches found in Fig. 4 are one of the possibilities identified in such an unfolding.

Equations (8) can also be used to describe the unfolding of the bifurcation at S_4 in Fig. 1. As before, this bifurcation splits into two successive bifurcations, labeled S_4 and S_4', that are too close to resolve in Fig. 4. Our calculations indicate that stable *x*-rolls bifurcate first, at S_4, as Ma decreases, followed by a branch of unstable *y*-rolls at S_4'. The former lose stability to a branch of stable asymmetric states at S_6, a result that is consistent with theory.[23] The theory also predicts that in this case there should be a small interval of stability on the latter branch due to a bifurcation to a branch of unstable asymmetric states that rejoins the branch almost immediately. We have been unable to locate this branch in the numerical calculations either because it is very short, or because it has already disappeared by the time A_x reaches $A_x=1.501$.

It remains to consider the other primary and secondary bifurcations present in Fig. 1. Except for their location, none of the remaining primary bifurcations is greatly affected by the changed symmetry since all are simple bifurcations: the bifurcation at P_2 remains a pitchfork because the associated eigenfunction (c) of Fig. 6 changes sign under both $\mathcal{S}_x$ and $\mathcal{S}_y$, the two generators of the symmetry group of a rectangle. The bifurcation at S_3 remains a pitchfork for identical reasons. Moreover, the bifurcation at T_1 respects the $\mathbf{D}_2$ symmetry of the container and hence remains transcritical. In contrast, the bifurcation at P_3 in Fig. 1 becomes the transcritical bifurcation T_2 in Figs. 4 and 5. This is because the associated eigenfunction (e) of Fig. 6 is invariant under both $\mathcal{S}_x$ and $\mathcal{S}_y$, i.e., it is unchanged under both generators of the symmetry $\mathbf{D}_2$ of the container. In a case like this, the symmetry $\mathbf{D}_2$ has no effect on the bifurcation and the bifurcation must therefore be generic, subject only to the requirement that the conduction solution is still a solution. Of course if ϵ is small enough the degree of transcriticality will be slight and hence barely visible. Finally, because of the trivial action of $\mathbf{D}_2$ on the solutions born at T_2 we also expect that the pitchfork bifurcation at S_5 should become an imperfect bifurcation, as observed in Figs. 4 and 5.

IV. CONCLUSIONS AND EXPERIMENTAL COMPARISONS

In this article we have described the various patterns expected of three-dimensional Marangoni convection in a small aspect ratio square container with realistic boundary conditions in a gravity-free environment. We have described how the $\mathbf{D}_4$ symmetry of the container affects the various primary and secondary bifurcations that take place as the Marangoni number Ma increases, and explained how these are in turn affected by breaking the symmetry from $\mathbf{D}_4$ to $\mathbf{D}_2$, i.e., making the container slightly rectangular. We anticipate that these considerations will be of great assistance in understanding other three-dimensional problems with square and nearly square symmetry, including, for example, Rayleigh–Bénard convection or the results of Dauby and

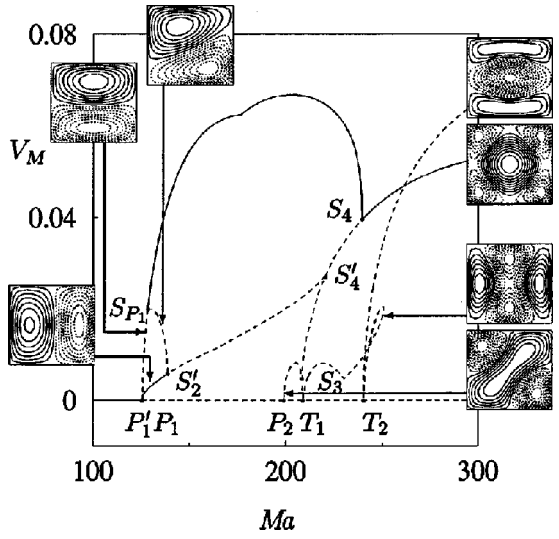

FIG. 7. Bifurcation diagram for $A_x=1.6$ and $A_y=1.5$. The resolution is $13\times13\times11$.

Lebon for the Marangoni–Bénard problem (e.g., Fig. 8 of Ref. 5). In the present case these considerations allow us to relate the structure of the bifurcation diagrams for more general rectangles such as that shown in Fig. 7 for $A_x=1.6$ and $A_y=1.5$ to that obtained for the square container. This is achieved by relating both to the intermediate bifurcation diagram shown in Fig. 4. This bifurcation diagram summarizes the properties of a *nearly square* container. We have described general principles that allow us to deduce the qualitative features of this diagram from that for the perfectly square container shown in Fig. 1. The resulting Fig. 4 may now be checked for consistency with the results summarized in Fig. 7. In this way it is possible to understand, for example, why the supercritical branch created at T_1 reconnects to the trivial state at another transcritical bifurcation at a larger value of Ma, a behavior seen in the two-dimensional case as well.[8] We can also understand the origin of the unstable branch $S_{P_1}-S_2'$ of near-diagonal states as a vestige of the unstable portion of the branch of Π-symmetric states present in the square container (Fig. 1). Note that for $A_x=1.6$ the stable portion of this branch, represented by S_2-S_6 in Fig. 4, has already disappeared.

We now summarize the predicted sequence of stable steady solutions which might be observable in an experiment with a slightly rectangular container $A_x\approx A_y=1.5$. For the perfect square case, $A=1.5$ (Fig. 1), several different flows can be observed: one-cell flows corresponding to *x*-rolls or *y*-rolls ($\mathcal{S}$-symmetric states), diagonal rolls along either diagonal (Π-symmetric states), as well as nonsymmetric rolls intermediate in form between these two. In addition multicellular flows in the form of a square pattern with upflow in the center ($\mathbf{D}_4$-symmetric state) can be stable. All these different patterns are observable in appropriate ranges of Ma: *x*-rolls and *y*-rolls in the same range, either close to the threshold (from P_1 to S_2) or from S_6 to S_4, diagonal rolls in a large intermediate range (from S_1 to S_7, a range almost equal to S_2-S_6), nonsymmetric rolls in a very narrow range (from S_2 to S_1), and finally the square patterns with upflow in the center beyond the point S_4 (Ma$\approx$246.3), the termination point of both the *x*- and *y*-roll branches. However, in the parameter range explored neither of the two possible $\mathbf{D}_2$-symmetric states was found to be stable.

When A_x is slightly increased ($A_x=1.501$, Fig. 4), the (now almost) square patterns with upflow in the center remain the only stable solutions beyond S_4. This point is now the termination point of the branch of *x*-rolls only. However, for the remaining flows even this small change in shape has a dramatic effect. This is because the primary bifurcation from the conduction state, at P_1', is now to *y*-rolls. However, the *y*-rolls are only stable in a small range of Ma close to threshold, P_1' to S_2', a range that decreases as A_x increases. In contrast the *x*-rolls are observable only after a secondary bifurcation point S_{P_1} close to P_1, but there is a substantial region of bistability between these two states. The two ranges of stability of the *x*-rolls, S_{P_1} to S_2 and S_6 to S_4, broaden with increasing A_x and merge for $A_x<1.6$ (see Fig. 7). Thus even though they are not the first state to set in, with increasing A_x the *x*-rolls become the prevalent one-cell pattern. For slightly rectangular containers ($A_x=1.501$, Fig. 4) stable, almost diagonal flows can still be observed on a relatively large interval in Ma (almost from S_2 to S_6 in Fig. 4), but this interval disappears rapidly as A_x increases, and for $A_x=1.6$ it is absent entirely (see Fig. 7). Thus, for containers with $(A_x-A_y)/A_x\approx6\%$ the most easily observable flows are the *x*-rolls and an almost square pattern with upflow in the center, while for $(A_x-A_y)/A_x\approx0.06\%$, several other one-cell patterns are readily observable as well. These results are at variance with the basic premise of Ref. 5 that containers with $(A_x-A_y)/A_x\approx1\%$ behave like square containers.

It is of interest to compare our results with experimental results on Bénard–Marangoni convection in square containers.[25,26] Although in these experiments the heat flux q is not constant and buoyancy forcing (as measured by a finite Rayleigh number) is present, our calculations are broadly consistent with the observations. For nominally square containers with $A=1.82$, Koschmieder and Prahl[25] find a square pattern when Ma=380 and Ra=228, where Ra is the Rayleigh number. This observation may be compared with our prediction that square patterns should be observed for Ma $>$246.3 when $A=1.5$ and Ra=0. For larger values of A, Koschmieder and Prahl find more complicated albeit regular patterns. For example, when $A=5.68$, Ma=54, and Ra=33, they find a $\mathbf{D}_2$-symmetric two cell state in which the fluid descends along the periphery of the container as well as along one diagonal. A solution of this type has the same symmetry as the solutions along the branch that bifurcates at P_2 for our parameter values, although our is unstable. Likewise, the three-cell state observed when $A=6.18$, Ma=80, and Ra=42 has the symmetry Π and, as a result, may be identified with the branch S_1-S_7 in Fig. 1. Indeed, it is not hard to believe that, as the aspect ratio increases, the computed solution could develop into the one observed. Thus the symmetry of the observed patterns is consistent with that of some of the computed patterns. Moreover, the presence of bistability in Fig. 1 is consistent with the observation of stable two-cell and three-cell states at $A=4.98$. More de-

tailed comparisons of the type attempted in Ref. 5 must, however, await larger aspect ratio calculations.

In contrast, the experiments reported in Ref. 26 are for $A=4.46$ and reveal a primary bifurcation to a steady $\mathbf{D}_4$-symmetric state, followed by a secondary bifurcation to a steady Π-symmetric state. From a symmetry point of view the former bifurcation is the same as T_1 in Fig. 1 while the latter corresponds to the point S_3. The theory described here indicates that the former bifurcation should be transcritical (a fact not mentioned in Ref. 26), with the latter a pitchfork. This bifurcation will remain a pitchfork in a rectangular container. These facts are unrelated to the ''hidden'' symmetries invoked by the authors of Ref. 26, which would, in any case, be broken by the no-slip lateral boundaries.

ACKNOWLEDGMENTS

The work of E.K. was supported in part by NASA Grant No. NAG3-2152. The authors wish to thank Dr. L. S. Tuckerman from the LIMSI (Orsay, France) for fruitful discussions, and a referee for bringing Ref. 25 to their attention.

[1] S. M. Pimputkar and S. Ostrach, ''Convective effects in crystal growth from melt,'' J. Cryst. Growth **55**, 614 (1981).
[2] S. Rosenblat, G. M. Homsy, and S. H. Davis, ''Nonlinear Marangoni convection in bounded layers. Part 2. Rectangular cylindrical containers,'' J. Fluid Mech. **120**, 123 (1982).
[3] H. A. Dijkstra, ''On the structure of cellular solutions in Rayleigh–Bénard–Marangoni flows in small-aspect-ratio containers,'' J. Fluid Mech. **243**, 73 (1992).
[4] H. A. Dijkstra, ''Surface tension driven cellular patterns in three-dimensional boxes—Linear stability,'' Microgravity Sci. Technol. **7**, 307 (1995); ''Part II: A bifurcation study,'' *ibid.* **8**, 70 (1995).
[5] P. C. Dauby and G. Lebon, ''Bénard–Marangoni instability in rigid rectangular containers,'' J. Fluid Mech. **329**, 25 (1996).
[6] A. Bergeon, D. Henry, and H. Ben Hadid, ''2D and 3D Marangoni pattern selection in shallow cavities,'' Adv. Space Res. **8**, 1223 (1998).
[7] A. Bergeon, D. Henry, and H. Ben Hadid, ''Instabilité de Marangoni–Bénard,'' in Proc. 14eme Congrès Francais de Mécanique, Toulouse, France (1999).
[8] A. Bergeon, D. Henry, H. BenHadid, and L. S. Tuckerman, ''Marangoni convection in binary mixtures with Soret effect,'' J. Fluid Mech. **375**, 143 (1998).
[9] A. T. Patera, ''A spectral element method for fluid dynamics: Laminar flow in a channel expansion,'' J. Comput. Phys. **54**, 468 (1984).
[10] G. Em. Karniadakis, M. Israeli, and S. A. Orszag, ''High-order splitting method for the incompressible Navier–Stokes equations,'' J. Comput. Phys. **97**, 414 (1991).
[11] L. S. Tuckerman, ''Steady-state solving via Stokes preconditioning: Recursion relations for elliptic operators,'' in *Proceedings of the 11th International Conference on Numerical Methods in Fluid Dynamics*, edited by D. L. Dwoyer, M. Y. Hussaini, and R. G. Voigt (Springer-Verlag, New York, 1989).
[12] C. K. Mamun and L. S. Tuckerman, ''Asymmetry and Hopf bifurcation in spherical Couette flow,'' Phys. Fluids **7**, 80 (1995).
[13] A. Bergeon and D. Henry, ''A continuation method applied to the study of three dimensional Rayleigh–Bénard and Marangoni–Bénard instabilities,'' in *Continuation Methods in Fluid Dynamics*, edited by D. Henry and A. Bergeon, *Notes on Numerical Fluid Mechanics* 74 (Vieweg, Braunschweig/Wiesbaden, 2000).
[14] C. Canuto, M. Hussaini, A. Quarteroni, and T. A. Zang, *Spectral Methods in Fluid Mechanics* (Springer-Verlag, New York, 1987).
[15] This terminology is opposite to that used by S. H. Davis, ''Convection in a box: Linear theory,'' J. Fluid Mech. **30**, 465 (1967).
[16] J. D. Crawford and E. Knobloch, ''Symmetry and symmetry-breaking bifurcations in fluid dynamics,'' Annu. Rev. Fluid Mech. **23**, 341 (1991).
[17] M. Golubitsky and M. Roberts, ''A classification of degenerate Hopf bifurcations with $\mathbf{O}(2)$ symmetry,'' J. Diff. Eqns. **69**, 216 (1987). This classification is relevant here because the equations for the amplitudes of left- and right-traveling waves obtained from the normal form for the $\mathbf{O}(2)$-symmetric Hopf bifurcation have $\mathbf{D}_4$ symmetry. This observation is due to J. W. Swift, Ph.D. thesis, University of California at Berkeley, 1984.
[18] M. Golubitsky, I. Stewart, and D. G. Schaeffer, *Singularities and Groups in Bifurcation Theory* (Springer-Verlag, New York, 1988), Vol. 2.
[19] For a discussion of these representations in a fluid dynamical context, see A. M. Rucklidge, N. O. Weiss, D. P. Brownjohn, P. C. Matthews, and M. R. E. Proctor, ''Compressible magnetoconvection in three dimensions: Pattern formation in a strongly stratified layer,'' J. Fluid Mech. **419**, 283 (2000).
[20] E. Knobloch, ''On the degenerate Hopf bifurcation with $\mathbf{O}(2)$ symmetry,'' Contemp. Math. **56**, 193 (1986).
[21] The classification of the $\mathbf{D}_4$-symmetric steady state bifurcation in Refs. 17 and 18 uses contact equivalence. This type of equivalence does not preserve the stability of the nonsymmetric solutions (a_1,a_2), $a_1 \neq a_2$, if these are not saddles (see Ref. 17, proposition 3.2).
[22] S. van Gils and J. Mallet-Paret, ''Hopf bifurcation and symmetry: Travelling and standing waves on the circle,'' Proc. R. Soc. Edinburgh, Sect. A: Math. **104**, 279 (1986).
[23] J. D. Crawford and E. Knobloch, ''On degenerate Hopf bifurcation with broken $\mathbf{O}(2)$ symmetry,'' Nonlinearity **1**, 617 (1988).
[24] M. Golubitsky, I. Stewart, and D. G. Schaeffer, *Singularities and Groups in Bifurcation Theory* (Springer-Verlag, New York, 1985), Vol. 1.
[25] E. L. Koschmieder and S. A. Prahl, ''Surface-tension-driven Bénard convection in small containers,'' J. Fluid Mech. **215**, 571 (1990).
[26] G. B. Mindlin, T. Ondarçuhu, H. L. Mancini, C. Pérez-García, and A. Garcimartín, ''Comparison of data from Bénard–Marangoni convection in a square container with a model based on symmetry arguments,'' Int. J. Bifurcation Chaos Appl. Sci. Eng. **4**, 1121 (1994).